Damping and mechanical behaviour of composite laminates interleaved with rubbery nanofibers

Damping and mechanical behaviour of composite laminates interleaved with rubbery nanofibers

Marco Povolo[a]*, Emanuele Maccaferri[b], Davide Cocchi[a], Tommaso M. Brugo[a], Laura Mazzocchetti[b], Loris Giorgini[b], Andrea Zucchelli[a]

[a]Department of Industrial Engineering, University of Bologna, Viale Risorgimento 2, 40136 Bologna, Italy

[b]Department of Industrial Chemistry "Toso Montanari", University of Bologna, Viale Risorgimento 4, 40136 Bologna, Italy

Abstract

The development of composite components with superior damping capacity is welcome in fields like automotive and aerospace for improving comfort and reducing composite damages. Here, a structural composite with improved damping and unaffected overall mechanical properties is presented. Vibration hampering is achieved by interleaving electrospun Nitrile Butadiene Rubber / poly(ϵ-caprolactone) (NBR/PCL) blend nanofibrous mats into epoxy unidirectional Carbon Fiber Reinforced Polymer (CFRP) prepregs. Three laminate configurations were produced using rubbery nonwoven layers with different thicknesses (5, 10 and 20 μm) for evaluating the effect of grammage layer on CFRP damping and mechanical properties. A preliminary thermomechanical behaviour of modified CFRPs was evaluated via Dynamic Mechanical Analysis (DMA), while the influence of both interleaved mat grammage and testing temperature was more deeply investigated via destructive three-point bending (3PB) analyses. Flexural elastic modulus and strength of rubbery-modified CFPSs are comparable to unmodified laminate. Some lowering occurs only at relatively high temperature when present the highest mat grammage.

Damping behaviour was evaluated by single cantilever beam vibration tests using the advanced Modified-Coulomb-Model (MCM). The interleaved NBR/PCL mats improved the composite damping up to +77 %, without significantly affecting the laminate mechanical properties, weight, and thickness.

Keywords: Damping, nanofibers, composite laminates, rubber, electrospinning, CFRP.

***Corresponding Author:** Marco Povolo, Department of Industrial Engineering, University of Bologna, 40132 Bologna, Italy. Mail: marco.povolo2@unibo.it, Phone: +39 340 8316493

1. Introduction

Fiber Reinforced Polymers (FRPs) have many advantages over traditional materials mainly because of their favourable specific stiffness, specific strength, and the capacity of dissipating energy. These characteristics make composite laminates suitable for high-performance applications like aerospace, automotive, industrial, sport, etc. Traditional materials, like metals, have low damping capabilities resulting in high amplitude vibrations that can cause damages to structures [1]. FRP laminates, on the other hand, show higher damping properties than traditional ones. At the micromechanical level, the energy dissipation is induced by different phenomena such as the viscoelasticity of the matrix, the damping of fibers and matrix, their interfaces, or by damages [2]. At the laminate level, instead, damping depends on the layer orientations, stacking sequence, and interlaminar effects [3]–[5].
The fiber type also influences the damping value of the composite. Kevlar fiber composites show a greater damping power compared to glass and carbon fiber ones [3], [6]. Instead, the addition of flax fibers to carbon fiber provides good damping behaviour, but the mechanical properties of the hybrid composite quickly decay as the flax fiber content increases [4].

The matrix nature also impacts on the final composite performance. Thermoplastic matrix confers to FRPs higher damping respect to thermosets, like epoxy resin, but the overall composite mechanical properties are poor, making thermoplastics not suitable for structural applications [7]. A common solution to increase the damping capacities of composite materials is the integration of bulk viscoelastic layers between FRP plies [1], [8], [9]. The damping enhancement using viscoelastic layers appears to be an effective, constructively simple, and low-cost solution. However, their integration compromises the overall stiffness and strength of the laminate besides causing an increase in its weight and size [10].

A novel method to increase the dynamic performance of composite laminates is to integrate nano-reinforcements into the matrix, like nanoparticles [11], [12] carbon nanotubes (CNTs) [13]–[15], and nanofibers [16]. CNTs offer a greater surface to volume ratio interfaces than classic fibers, enhancing the damping behaviour of the hosting composite laminate [13], [15], [17]. Thermoplastic nanofibers are also used for hindering delamination by increasing the interlaminar fracture toughness [16], but may not significantly improve damping properties [18], [19]. On the contrary, elastomers may positively contribute to the damping enhancement, thanks to their intrinsic viscoelastic nature [20]. Few attempts to obtain rubbery nanofibers are reported in the literature due to difficulties in their production, arising from the rubber cold flow which leads to the formation of a compact bulk film. Usually, papers report just the proof of concepts of the possibility to electrospin rubber polymeric solutions [21]–[24], or they attain microfibers rather than nanofibers [25], [26]. Often, rubbery nanofibers need to be crosslinked for avoiding nanofiber coalescence [27]. The rubber cold flow phenomenon may be so important that the crosslinking step has to be applied during electrospinning [28] or immediately after the process [25], [29], thus strongly limiting the obtainable final membrane thickness. Recently, the production of rubbery nanofibers by single-needle electrospinning of polymeric blends made of Nitrile Butadiene Rubber and poly(ϵ -caprolactone) (NBR/PCL) was reported by Maccaferri *et al*. [30]. This method allows producing rubbery nanofibers with a high amount of NBR fraction without the need for a crosslinking step: the

nanofibrous morphology is stable at room temperature, and there are no restrictions to the obtainable mat thickness. The same rubbery nanofibrous mats were successfully interleaved in Carbon Fiber Reinforced Polymer (CFRP) epoxy laminates, resulting in the first reported work on CFRP laminates modified with rubbery nanofibers [18]. The Authors found up to +480 % of Mode I energy release rate, in addition to an impact on the overall composite thermomechanical properties which has to be further investigated.

In this work, an advanced structural composite with improved damping is presented, by interleaving NBR/PCL blend nanofibrous mats into unidirectional epoxy-based CFRPs. A preliminary thermomechanical behaviour of modified CFRPs was evaluated via Dynamic Mechanical Analysis (DMA), while the influence of both interleaved mat grammage and testing temperature was more deeply investigated via destructive three-point bending (3PB) analyses. Damping behaviour was assessed via single cantilever beam vibration tests. To perform an accurate measurement of damping and separating the damping contribution of the air and the joint from the contribution of the material, the advanced Modified Coulomb Damping (MCD) model was adopted [31], [32]. Moreover, mechanical properties were evaluated as a function of temperature performing three-point bending (3PB) tests.

2. Materials and Methods

Electrospinning

Carboxylated nitrile butadiene rubber (NBR) NIPOL 1072CGX was purchased from Zeon Chemicals (68 %mol butadiene, 28 %mol acrylonitrile, 4 %mol methacrylic acid). Poly(ε-caprolactone) (PCL), M_w 70,000-90,000, was purchased from Sigma-Aldrich. Polymers were both used without any preliminary treatment. N,N-dimethylacetamide (DMAc), N,N-dimethylformamide (DMF) and chloroform ($CHCl_3$) were purchased from Sigma-Aldrich and used without further purifications.

Rubbery NBR/PCL nanofibrous mats were prepared following the method proposed by Maccaferri *et al.* [30]. NBR solution (S-NBR, 10 %wt) was prepared in DMAc (e.g., 1.0 g of polymer in 9.6 mL of solvent) under magnetic stirring at room temperature until the formation of a homogeneous solution. PCL solution (S-PCL, 10 %wt) was prepared in $CHCl_3$ / DMF 1:1 wt (e.g., 1.0 g of polymer in 3.0 mL of $CHCl_3$ and 4.8 mL of DMF) under magnetic stirring at room temperature until complete polymer solubilization. NBR/PCL blend was prepared by mixing 60 %wt of S-NBR and 40 %wt of S-PCL solutions. The polymer blend was stirred for a minimum of 2 h to ensure proper homogenization. Nanofibrous mats (named *n*-60/40) were produced using a Spinbow® electrospinning machine equipped with four 5 mL syringes. Needles (length 55 mm, internal diameter 0.84 mm) were joined to syringes via Teflon tubing. Nanofibers were collected on a drum covered with poly(ethylene)-coated paper rotating at 50 rpm (tangential speed 0.39 m/s). Mats had final dimensions of approximately 30 × 40 cm. To achieve different nanofiber thicknesses/grammages, only the electrospinning time was changed. The electrospinning process parameters and environmental conditions are reported in Table 1.

Table 1 – Electrospinning process parameters and nanofibers diameter.

Nanofibrous mat	Flow rate	Electric potential	Distance	Electric field[(a)]	Temperature	Relative humidity	Nanofibers diameter[(b)]
	mL/h	kV	cm	kV/cm	°C	%	nm
n-60/40	0.55	18.3	13	1.4	22-24	20-22	268 ± 43

[(a)] calculated as electric potential to distance ratio

[(b)] as spun nanofiber

To assess the thickness of the nanofibrous layers, a digital comparator (Alpa MegaRod) was used. To calculate the mat grammage (i.e., the mat weight per square meter), the nanofibrous layers were weighted by a scale with a resolution of 0.01 mg (Radwag AS 60/220.R2). Nanofiber morphology (Figure 1) was observed through a Scanning Electron Microscope (SEM, Phenom ProX).

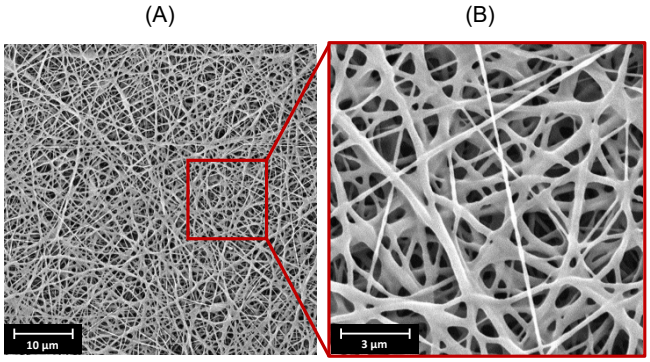

Figure 1 – SEM micrographs of NBR/PCL rubbery nanofibrous mat (n-60/40) at (A) 5,000x magnification and (B) 20,000x magnification.

Laminates and specimens fabrication

The carbon fiber epoxy unidirectional prepreg was T700S-24K/DT210 epoxy-based resin provided by Deltapreg (Toray group, Italy), with V_f = 53 % and 350 g/m^2 of carbon fibers.

Four laminate configurations, reported in Table 2, were fabricated by staking 7 layers of unidirectional prepreg all oriented at 0°. A reference configuration composed of only prepreg plies without interleaved layers (named ref.) and three nano-structured ones with 5 µm, 10 µm, and 20 µm thick nanofibrous layers interleaved at each prepreg interface (named int. 5, int. 10, and int. 20, respectively) were produced.

Table 2 – Configurations of produced sample laminates.

Configuration	Mat thickness	Mat grammage
	µm	g/m^2
ref.	-	-
int. 5	5	2.5
int. 10	10	5.1
int. 20	20	9.6

Laminates were cured with vacuum bag technology in autoclave at 130 °C for 2 hours and 6 bar pressure. The resulting laminates thickness was 2.6 mm without significant difference among laminates configurations. For each configuration, the specimens for thermomechanical (DMA), mechanical (3PB) and dynamic (damping) tests were extracted from the same laminate. Their

dimensions, defined according to ASTM D7264, ISO 6721-1 and ASTM E756-05, are reported in Table 3.

Table 3 – Specimens geometry.

Test	Length mm	Width mm	Thickness mm
DMA	50	7.5	2.6
3PB	110	15	2.6
Damping	280	25	2.6

Thermomechanical, mechanical, and damping tests

Overall thermomechanical properties of CFRPs were evaluated via DMA, using a Netzsch DMA 242 E Artemis instrument in a three-point bending configuration with a fixed span of 40 mm. DMA analyses were carried out with a heating ramp from 0 to 170 °C, 3 °C/min heating rate, 1 Hz oscillating frequency, 20 μm amplitude and a static / dynamic force ratio of 1.5. For each laminate configuration 3 specimens were tested.

Flexural tests were carried out to assess the effect of the nanofibrous rubbery membranes on the mechanical properties of the different laminate configurations. Two different types of flexural tests under different conditions were performed: i) the destructive one, carried out until failure, to evaluate the elastic modulus and the flexural strength at three different temperatures (20, 50, and 80 °C) and ii) a dynamic test performed in the elastic regime at a frequency of 1 Hz to evaluate the elastic modulus degradation as a function of the temperature. Regarding type i) 3PB test, the aforementioned temperatures were chosen because 20 °C is the reference RT, 50 °C because it is slightly lower than the melting of the PCL crystalline fraction of the rubbery blend, and 80 °C because it is enough above the PCL melting temperature. Type ii) 3PB test, despite similar to the DMA one, allowed a more precise assessment of the flexural modulus as a function of the temperature. In fact, since UD CFRP laminates exhibit a very high flexural stiffness, the evaluation of storage modulus (E') by the DMA may be not accurate. 3PB tests were performed on Instron

Model 8033 equipped with a climatic chamber using a 2 kN load cell. The destructive tests were conducted at a crosshead speed of 2 mm/min. The dynamic ones were sinusoidally loaded between 0.15 % and 0.30 % maximum flexural strain amplitude. A total of 12 3PB specimens were tested for each laminate configuration.

The dynamic tests for damping evaluation were performed according to ASTM E756-05 in a cantilever beam configuration with a laser sensor (optoNCDT 1402 - Micro-Epsilon) pointed at the specimen tip, as shown in Figure 2. The specimen was excited by preloading its tip and then instantaneously releasing it. For each laminate configuration, 3 specimens were tested and for each one 5 repetitions were performed. The setup parameters, depicted in Figure 2, were L = 255 mm, d = 105 mm, C = 25 Nm, a = 5 mm.

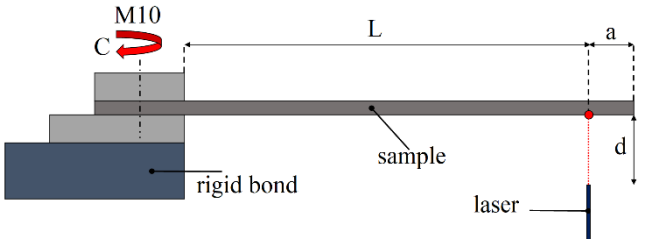

Figure 2 – Damping test setup scheme.

The tip displacement measured by the laser was acquired at 2 kHz by ADC converter (NI-9215 National Instruments) and processed by a MATLAB custom software based on MCD model. First, the signal was cut with a 10 s time window (Figure 3A). Subsequently, the Short Time Fourier Transform (STFT) was performed to obtain the spectrogram of the signal. In Figure 3B each curve represents the amplitude vs frequency for a specific time segment of the signal. The STFT was performed in MATLAB by using the *spectrogram* function. The signal was cut into time segments 0.1 s long, by using the Hamming window function. Then, each signal segment was extended on 1 s time span by using the zero-padding technique, in order to increase the frequency resolution of the Fast Fourier Transform (FFT). A high signal segment overlap of 15/16 was chosen to have a high time resolution. The aforementioned parameters have been experimentally optimized for the specific type of signal analysed in this work.

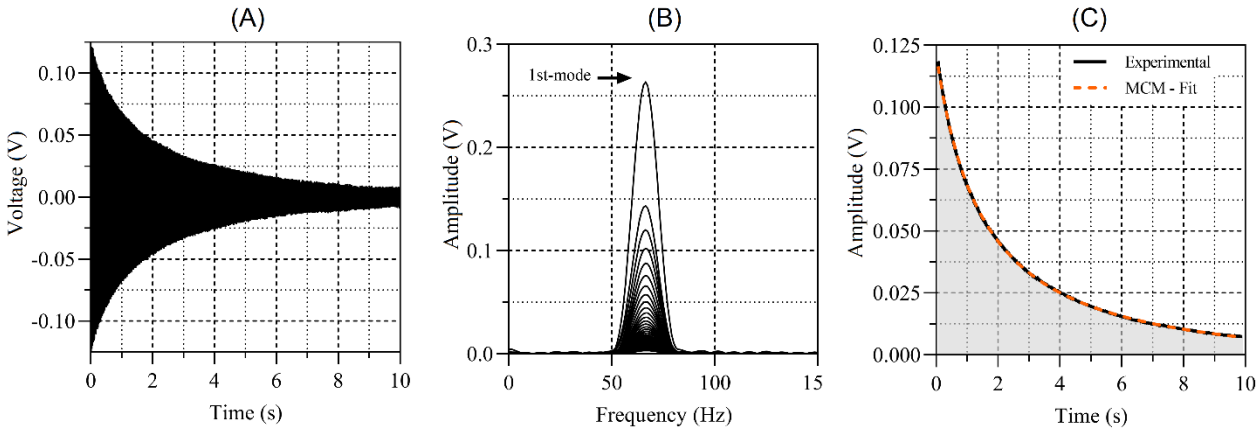

Figure 3 – (A) Original signal acquired by laser sensor; (B) Short Time Fourier Transform (STFT) of the signal; (C) Experimental amplitude decay as a function of time and fitting with the Modified-Coulomb-Damping (MCD) model.

Then, for each amplitude vs frequency curve of the STFT of Figure 3B, the maximum amplitude of the first resonance frequency was extracted and expressed as function of time (Figure 3C). In this way, it was possible to find the amplitude decay curve in the time domain.

According to the Modified Coulomb Damping (MCD) model [32] the time varying amplitude can be defined as:

$$\dot{y}(t) = -c - by(t) - ay(t)^2 \qquad \text{Eq. 1}$$

where t is the time and a, b and c are coefficients accounting for viscous (air), material (structural or hysteretic) and Coulomb (friction) damping contributions, respectively. Solving the first-order Eq. 1, under the assumption that the Coulomb damping is not dominant (i.e. $4ac < b^2$), the amplitude can be expressed as:

$$y(t) = \frac{b(p-1) + r(p+1)}{2a(1-p)} \qquad \text{Eq. 2}$$

where $r = (b^2 - 4ac)$, $\alpha = 2ay_0 + b - r$, $\beta = 2ay_0 + b + r$, $p = {}^{\alpha}/_{\beta} e^{-rt}$ and y_0 the initial amplitude. Eq. 2 was fitted on the experimental amplitude decay curve using the robust regression

with least absolute residuals weight function. In this way it was possible to separate the material damping contribution (coefficient b) from the air and friction ones.

An equivalence with the well-known classic damping ratio ζ can be done assuming that the material damping contribution is dominant. Hence, the MCD time varying amplitude (Eq. 1) can be simplified as $\dot{y}(t) = -by(t)$. The solution of this first-order equation is:

$$y(t) = y_0 e^{-bt} \qquad \text{Eq. 3}$$

In the same manner, it is possible to express the response of the well-known single-degree of freedom mass-springer-damper model (given by $m\ddot{x}(t) + c\dot{x}(t) + kx(t) = 0$) as $x(t) = x_0 e^{-\zeta\omega_n t} \cos(\omega_n\sqrt{1-\zeta^2})$ or in terms of amplitude as:

$$y(t) = y_0 e^{-\zeta\omega_n t} \qquad \text{Eq. 4}$$

where ω_n is the resonance frequency. Finally, matching the amplitude of the MCD model (Eq. 3) with the one of the classical single-degree of freedom mass-spring-damper model (Eq. 4), it is possible to express the equivalent damping ratio as:

$$\xi = \frac{b}{\omega_n} \qquad \text{Eq. 5}$$

3. Results

Thermomechanical characterization

An overview of the overall thermomechanical properties of the different laminate configurations was evaluated via DMA. In Figure 4 the storage modulus (E') and loss factor ($tan\delta$) versus temperature are plotted. The laminates int. 5 and int. 10 show an E' trend similar to the reference one. The storage modulus is comparable to the one displayed by the unmodified CFRP, while the E' onset slightly lowers (107 °C vs 113 °C for the ref.). By contrast, int. 20 shows a first E' onset at 55

°C, and a main *E'* drop characterized by an onset at 99 °C. The first onset can be attributed to the melting of the PCL crystalline fraction, while the second drop is due to the glass transition of the toughened epoxy resin. The behaviour of the last sample is similar to what evidenced by a previous study [30].

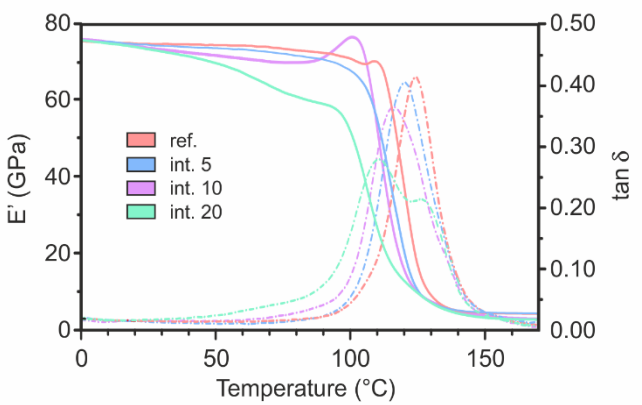

Figure 4 – DMA analyses of the different laminate configurations.

Regarding the *tanδ*, the peaks do not show relevant shifts for increasing grammage of interleaved mats, except for int. 20 configuration (main peak at 111 °C vs 124 °C for the ref. one). Besides, the shape of the curve is different, displaying two peaks. The first peak accounts for the toughened epoxy resin thanks to mixing with NBR/PCL blend, while the second one, at 128 °C, is due to the unmodified resin fraction. It is worth mentioning that in almost all the modified laminates, the presence of the NBR/PCL blend widens the window dissipation energy of the composite to lower temperatures, indicating a potentially damping enhancement also at room temperature.

Mechanical tests and fracture analysis

The influence of both interleaved mat grammage and temperature was more deeply investigated via destructive 3PB analyses. Flexural elastic modulus and strength of the different sample configurations do not evidence significant differences at RT (Figure 5), which stay near 100 GPa and 1100 MPa, respectively. However, with increasing temperature, the effect of the nanomat becomes more noticeable, especially for higher mat grammages. Indeed, at 80 °C the int. 20

configuration shows a reduction of 13 % in elastic modulus and 20 % in flexural strength compared to the ref. configuration. These results agree with the overall performance of E' identified by the DMA tests.

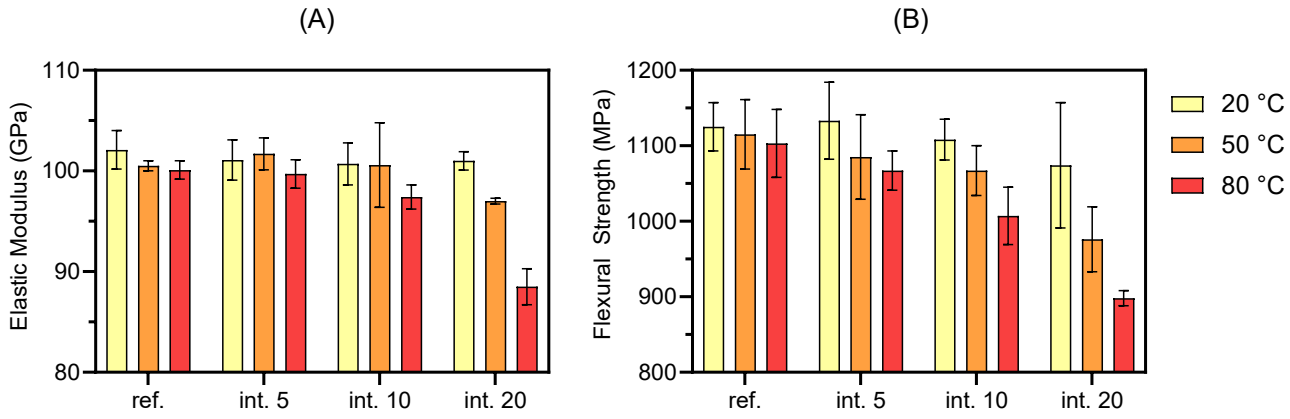

Figure 5 – (A) Flexural elastic modulus and (B) flexural strength for different sample configurations and temperatures.

The variation of laminate elastic modulus upon temperature was deeply elucidated carrying out 3PB cyclic loading-unloading tests. Figure 6 shows the flexural modulus as a function of temperature. As can be noticed, the elastic modulus shows a significant reduction only when high temperatures (> 80 °C) and high grammages (> 5 g/m^2, int. 10) are combined. However, during the life-cycle of common composite components, these high temperatures are rarely reached, except for special applications.

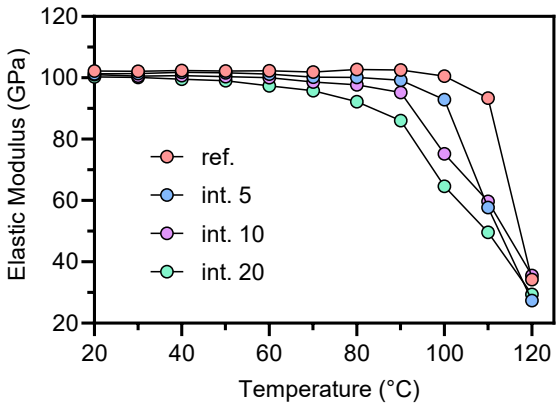

Figure 6 – Temperature dependence of flexural modulus.

Although the qualitative trends of E' and flexural modulus are similar, the numerical values shown in Figure 6 are much more reliable than those obtained from the DMA, where E' is strongly

influenced by the specific specimen loading region (e.g., local fiber/matrix ratio under solicitation). On the contrary, since the imposed deformation in 3PB test is macroscopic, the local effects become negligible because the stressed volume is increased.

In Figure 7 are displayed the perpendicular and parallel views of the fracture surfaces of 3PB specimens tested up to failure at RT for each laminate configuration. In this way, it was possible to observe both pulled out fibers (in blue in the sketch of Figure 7) and fibers broken in correspondence of the fracture surface of the specimen (in red). Moreover, int. 20 was analysed also at 50 and 80 °C.

The fracture surfaces of the ref. laminate appear sharp and brittle, with a marked fiber/matrix debonding (perpendicular view) and naked pulled out carbon fibers (parallel view). This behaviour is typical of low-toughened thermosetting polymers.

For nano-interleaved laminates, it can be noticed that the nanofibrous morphology is completely lost. Indeed, as previously observed in Figure 7, during the curing cycle the NBR/PCL blend mixed with the epoxy resin, leading to toughened matrix. As a matter of fact, by increasing the grammage of interleaved mat, the fracture surfaces become more irregular with more pronounced indented markings, meaning a greater ductile deformation. Moreover, a higher adhesion between carbon fibers and toughened epoxy matrix (perpendicular view) is found, and the matrix remains attached to the pulled out fibers (parallel view). This effect is maximized in int. 20, particularly when the testing temperature is increased from RT to 50 and 80 °C.

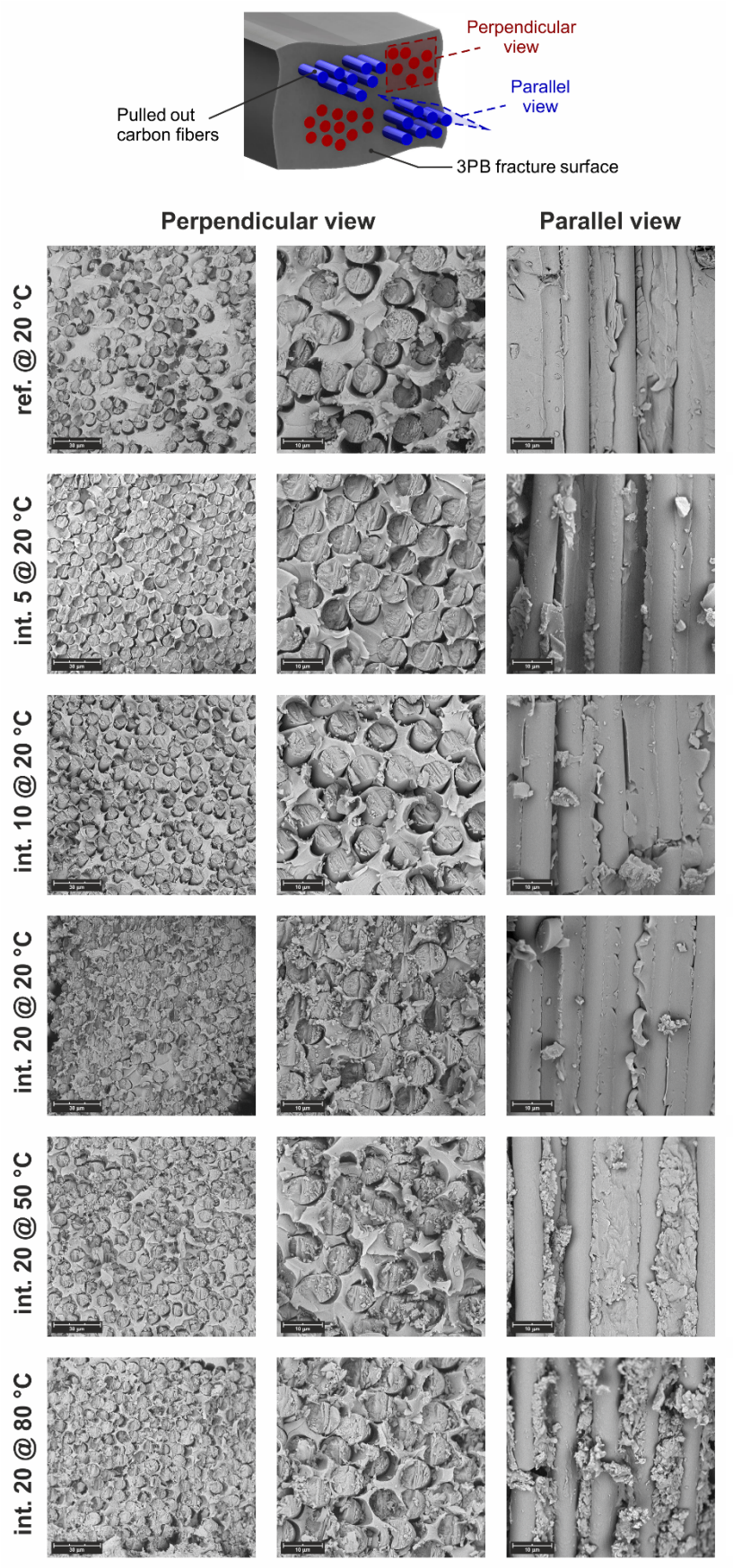

Figure 7 – SEM micrographs of 3PB specimens after destructive tests (magnification: first column 2,000x; second and third columns 5,000x).

Damping Analysis

Regarding damping tests, the fitting of the experimental signal with MCD model has always guaranteed a $R^2 \geq 0.99$. It was therefore possible to calculate the normalized material damping value for each configuration by excluding the contribution of both air and joint friction. This method was adopted because the damping effect of the air is predominant compared to the material one.

The material damping factor ranges from $1.75 \cdot 10^{-3}$ to $3.10 \cdot 10^{-3}$ for the ref. and int. 20 configurations, respectively (Figure 8A). Figure 8B shows the material damping enhancement versus the laminate weight variation for the different configurations. It is interesting to note that as the grammage of the nanofibrous membranes increases an exponential trend is observed in material damping. The major damping enhancement was obtained with the int. 20 configuration, achieving an improvement of 77 % for a laminate weight increment of 1.5 % only.

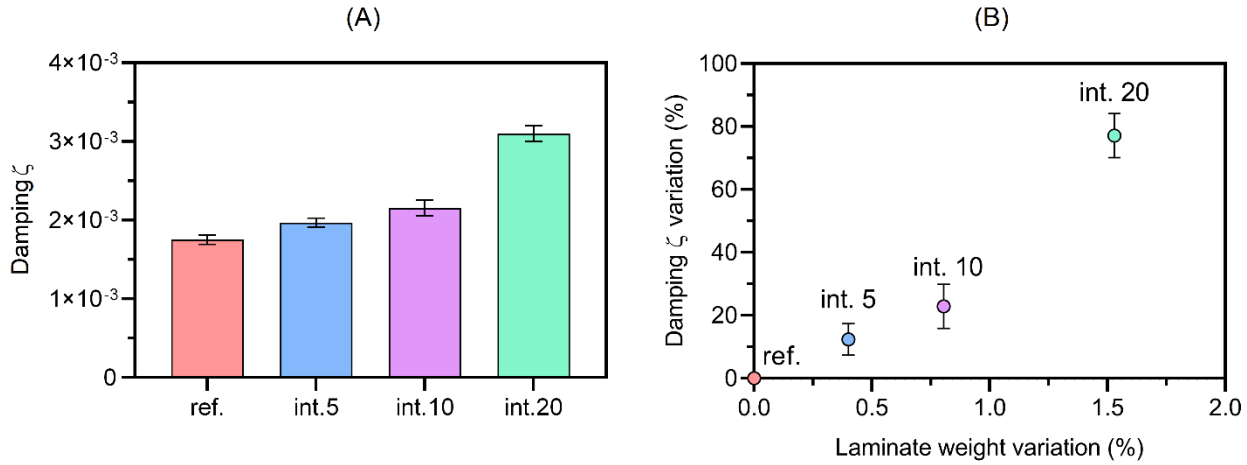

Figure 8 – (A) Material damping of the different sample configurations and (B) material damping percentage variation as a function of the laminate percentage weight variation.

4. Conclusions

In this work a structural composite was prepared by interleaving rubbery NBR/PCL nanofibrous layers between unidirectional CFRP prepreg laminates.

Thermomechanical properties were experimentally evaluated using 3PB tests and DMA. Flexural tests show no significant differences at room temperature in elastic modulus and flexural strength

between reference and nano-modified configurations. Only for the highest grammage and for temperatures over 50 °C, the effect of the nanomat becomes noticeable. In particular, when 80 °C are reached, the int. 20 configuration shows a reduction of 13 % in elastic modulus and 20 % in flexural strength compared to the ref. one. These results are in good accordance with DMA ones, which shows an *E'* onset drop from 113 °C to 55 °C. The morphology of the fracture surfaces as well appears to be affected by the amount of interleaved rubbery nanofibers, becoming more irregular and ductile.

Damping behaviour was evaluated by single cantilever beam vibration tests. Thanks to the advanced Modified-Coulomb-Damping (MCD) model, an accurate measurement of the material damping was obtained excluding the air and joint contributions.

The interleaved NBR/PCL nanofibrous mats greatly improved the composite damping capacity with a maximum increase of 77 % in the composite loss factor, with a negligible influence on flexural strength and modulus below *E'* onset temperature. Moreover, no significant impact on laminate weight and thickness, respect to reference samples without nano-reinforcement, were found. Hence, this type of nano-modified composite material is suitable for all those applications that require high energy dissipation ensuring at the same time high mechanical performance even at intermediate in-service temperature. The integration of nanofibrous rubbery membranes interspersed between the composite laminae overcomes the limits related to the use of bulk viscoelastic layers, which could negatively affect the laminate weight and integrity, even increasing its fracture toughness. This technique may allow engineers to design advanced composite components with high damping capacity by ultra-low grammage rubbery nanofibrous layers addition.

Acknowledgements

Authors wish to acknowledge the project POR-FESR 2019 - "*i-LBBox (Intelligent Lightweigth Battery Box*)" (No. E31B19000230009) and POR-FESR 2018 - "*TEAM SAVE*" (No. E91B18000460007) for financial support.

Data Availability

The raw/processed data required to reproduce these findings cannot be shared at this time as the data also forms part of an ongoing study.

Bibliography

[1] J. M. Berthelot, M. Assarar, Y. Sefrani, and A. El Mahi, "Damping analysis of composite materials and structures," *Compos. Struct.*, vol. 85, no. 3, pp. 189–204, 2008.

[2] A. D. Nashif, D. Jones, and J. Henderson, *Vibration damping*. 1985.

[3] J. M. Berthelot and Y. Sefrani, "Damping analysis of unidirectional glass and Kevlar fibre composites," *Compos. Sci. Technol.*, 2004.

[4] M. J. Le Guen, R. H. Newman, A. Fernyhough, G. W. Emms, and M. P. Staiger, "The damping-modulus relationship in flax-carbon fibre hybrid composites," *Compos. Part B Eng.*, vol. 89, pp. 27–33, 2016.

[5] A. Treviso, B. Van Genechten, D. Mundo, and M. Tournour, "Damping in composite materials: Properties and models," *Compos. Part B Eng.*, vol. 78, pp. 144–152, 2015.

[6] R. M. Crane and J. W. Gillespie, "Characterization of the vibration damping loss factor of glass and graphite fiber composites," *Compos. Sci. Technol.*, 1991.

[7] D. D. L. Chung, "Structural composite materials tailored for damping," in *Journal of Alloys and Compounds*, 2003.

[8] J. Li and Y. Narita, "Analysis and optimal design for the damping property of laminated

viscoelastic plates under general edge conditions," *Compos. Part B Eng.*, 2013.

[9] M. R. Maheri, "The effect of layup and boundary conditions on the modal damping of FRP composite panels," *J. Compos. Mater.*, 2011.

[10] H. Kishi, M. Kuwata, S. Matsuda, T. Asami, and A. Murakami, "Damping properties of thermoplastic-elastomer interleaved carbon fiber-reinforced epoxy composites," *Compos. Sci. Technol.*, 2004.

[11] B. B. Johnsen, A. J. Kinloch, R. D. Mohammed, A. C. Taylor, and S. Sprenger, "Toughening mechanisms of nanoparticle-modified epoxy polymers," *Polymer (Guildf).*, 2007.

[12] T. H. Hsieh, A. J. Kinloch, K. Masania, A. C. Taylor, and S. Sprenger, "The mechanisms and mechanics of the toughening of epoxy polymers modified with silica nanoparticles," *Polymer (Guildf).*, 2010.

[13] S. Tahan Latibari, M. Mehrali, L. Mottahedin, A. Fereidoon, and H. S. C. Metselaar, "Investigation of interfacial damping nanotube-based composite," *Compos. Part B Eng.*, 2013.

[14] N. A. Koratkar *et al.*, "Characterizing energy dissipation in single-walled carbon nanotube polycarbonate composites," *Appl. Phys. Lett.*, 2005.

[15] A. Montazeri and N. Montazeri, "Viscoelastic and mechanical properties of multi walled carbon nanotube/epoxy composites with different nanotube content," *Mater. Des.*, 2011.

[16] R. Palazzetti and A. Zucchelli, "Electrospun nanofibers as reinforcement for composite laminates materials – A review," *Composite Structures*. 2017.

[17] Y. Li, S. Cai, and X. Huang, "Multi-scaled enhancement of damping property for carbon fiber reinforced composites," *Compos. Sci. Technol.*, vol. 143, pp. 89–97, 2017.

[18] E. Maccaferri, L. Mazzocchetti, T. Benelli, T. M. Brugo, A. Zucchelli, and L. Giorgini, "Rubbery nanofibrous interleaves enhance fracture toughness and damping of CFRP laminates," *Mater. Des.*, 2020.

[19] C. Garcia, J. Wilson, I. Trendafilova, and L. Yang, "Vibratory behaviour of glass fibre reinforced polymer (GFRP) interleaved with nylon nanofibers," *Compos. Struct.*, 2017.

[20] Z. D. Xu, Y. X. Liao, T. Ge, and C. Xu, “Experimental and theoretical study of viscoelastic dampers with different matrix rubbers,” *J. Eng. Mech.*, 2016.

[21] X. Zhang and G. G. Chase, “Electrospun elastic acrylonitrile butadiene copolymer fibers,” *Polymer (Guildf).*, 2016.

[22] H. Wu, Q. Hu, L. Zhang, H. Fong, and M. Tian, “Electrospun composite nanofibers of polybutadiene rubber containing uniformly distributed Ag nanoparticles,” *Mater. Lett.*, 2012.

[23] X. Zhang, X. Yang, and G. G. Chase, “Filtration performance of electrospun acrylonitrile-butadiene elastic fiber mats in solid aerosol filtration,” *Sep. Purif. Technol.*, 2017.

[24] K. Phatcharasit, W. Taweepreda, K. Boonkerd, and J. K. Kim, “Electrospun epoxidized natural rubber with poly(vinyl chloride) (ENR-PVC) nanofibrous for PEMFC applications,” in *Advanced Materials Research*, 2014.

[25] M. W. Thielke, E. P. Bruckner, D. L. Wong, and P. Theato, “Thiol-ene modification of electrospun polybutadiene fibers crosslinked by UV irradiation,” *Polymer (Guildf).*, 2014.

[26] T. E. Kerr-Phillips *et al.*, “Electrospun rubber fibre mats with electrochemically controllable pore sizes,” *J. Mater. Chem. B*, 2015.

[27] M. Tian, Q. Hu, H. Wu, L. Zhang, H. Fong, and L. Zhang, “Formation and morphological stability of polybutadiene rubber fibers prepared through combination of electrospinning and in-situ photo-crosslinking,” *Mater. Lett.*, 2011.

[28] S. S. Choi, J. P. Hong, Y. S. Seo, S. M. Chung, and C. Nah, “Fabrication and characterization of electrospun polybutadiene fibers crosslinked by UV irradiation,” *J. Appl. Polym. Sci.*, 2006.

[29] H. Liu, B. Lin, and C. Jiang, “A new method for determining coal seam permeability redistribution induced by roadway excavation and its applications,” *Process Saf. Environ. Prot.*, 2019.

[30] E. Maccaferri, L. Mazzocchetti, T. Benelli, T. M. Brugo, A. Zucchelli, and L. Giorgini, “Rubbery nanofibers by co-electrospinning of almost immiscible NBR and PCL blends,” *Mater. Des.*, 2020.

[31] C. W. De Silva, *Vibration monitoring, testing, and instrumentation*. 2007.

[32] Clarence W. de Silva, *vibration and Shock handbook*. 2005.